

Efficient sunlight promoted nitrogen fixation from air under room temperature and ambient pressure via Ti/Mo composites¹

Liangchen Chen^a, Jingxuan Shou^b, Yutong Chen^a, Weihang Han^a, Xuwei Tu^a, Luping Zhang^a,

Qiang Sun^{c,†}, Jun Cao^a, Yurong Chang^d, Hui Zheng^{a,*}

^a College of Material, Chemistry and Chemical Engineering, Hangzhou Normal University,

Hangzhou 311121, P.R. China

^b College of civil Engineering, Zhejiang University of Technology, Hangzhou 311121, P.R. China

^c Australian Research Council Centre of Excellence for Nanoscale BioPhotonics (CNBP), School of Science, RMIT University, Melbourne, VIC 3001, Australia

^d Henan Qite New Material Co., Ltd., Zhengzhou 450000, P.R. China

[†] qiang.sun@rmit.edu.au

* huizheng@hznu.edu.cn

Abstract:

Photocatalytic nitrogen fixation is an important pathway for carbon neutralization and sustainable development. Inspired by nitrogenase, the participation of molybdenum can effectively activate nitrogen. A novel Ti/Mo composites photocatalyst is designed by sintering the molybdenum acetylacetonate precursor with TiO₂. The special carbon-coated hexagonal photocatalyst is obtained which photocatalytic nitrogen fixation performance is enhanced 16 times compared to pure TiO₂ at

¹ *Chemical Engineering Journal* **451** (2023) 138592, doi.org/10.1016/j.cej.2022.138592.

room temperature and ambient pressure. The abundant surface defects in this composite were confirmed to be the key factor for nitrogen fixation. The $^{15}\text{N}_2$ isotope labeling experiment was used to demonstrate the feasibility of nitrogen to ammonia conversion. Also, modelling on the interactions between light and the synthesized photocatalyst particle was examined for the light absorption. The optimum nitrogen fixation conditions have been examined, and the nitrogen fixation performance can reach up to $432 \mu\text{g}\cdot\text{g}_{\text{cat}}^{-1}\cdot\text{h}^{-1}$. Numerical simulations via the field-only surface integral method were also carried out to study the interactions between light and the photocatalytic particles to further confirm that it can be a useful material for photocatalyst. This newly developed Ti/Mo composites provide a simple and effective strategy for photocatalytic nitrogen fixation from air directly under ambient conditions.

Keywords: Photocatalytic nitrogen fixation; TiO_2 ; Room temperature and normal pressure; sunlight

1. Introduction

Ammonia supply is a key element in the economic chain in the world. Ammonia is not only the integral building block of amino acids and nucleotides, but also the crucial precursor in the synthesis of fertilizers, pharmaceuticals, and fibers.[1-3] It is well known that the greenhouse gas of ammonia industry is a major concern for sustainable development. Though 78% nitrogen in air is a handy source of raw material for ammonia industry, the big challenge is to activate nitrogen from its stable $\text{N}\equiv\text{N}$ triple bonds (941 kJ/mol).[4, 5] At present, the large-scale industrial nitrogen fixation is usually implemented via Haber-Bosch process to use nitrogen and hydrogen to synthesize ammonia under iron-based catalysts at high temperature and high pressure.[6] This process requires a large amount of fossil energy and emits a significant amount of carbon dioxide.[7-9] Therefore,

nitrogen fixation in a green way at room temperature and normal pressure has become one of the important research subjects in chemistry and chemical engineering.

In recent years, photo- and electro- catalysis have been regarded as promising methods of nitrogen fixation and have been widely studied due to their mild reaction conditions at room temperature and normal pressure.[10-15] In particular, photocatalytic nitrogen fixation is considered a more environment-friendly and eco-friendly method and more in line with sustainable development. Photocatalyst materials for nitrogen fixation have been studied including metal oxides, metal sulfides, g-C₃N₄, metal-organic frameworks (MOFs) and so on.[16-18] In the study of photocatalytic nitrogen fixation mechanism, an important aspect of semiconductor materials is the oxygen vacancies or other similar defect sites in the materials, and the signal peaks of oxygen vacancies are often characterized by ESR. For photocatalytic nitrogen fixation, the oxygen vacancies on the surface of the material are the active centers for enriching electrons and capturing nitrogen. The N≡N triple bond accepts the electrons provided by the oxygen vacancies and combines with the protons in the solution to form N-H bonds, which are finally converted into ammonia.[19, 20] For example, He *et al.* reported that indium sulfide nanotubes with more sulfur vacancies were prepared by calcining indium sulfide nanotubes to improve the photocatalytic nitrogen fixation effect.[21] Li and his group reported that the oxygen vacancy content increased and the photogenerated carrier separation and nitrogen adsorption capabilities of bismuth molybdate nanosheets were improved by etching bismuth molybdate with sodium hydroxide.[12]

TiO₂ is widely used in the field of photocatalysis, due to its stable chemical properties, photochemical stability, and electrons with strong reduction energy generated under illumination, which is often used for photodegradation of pollutants and water decomposition.[22] Anatase is a

common crystal form of TiO_2 and is an indirect semiconductor. The advantage of this structure is that the generated photoelectrons are not easy to recombine with holes and to annihilate. So it has bright prospects in the field of photocatalytic nitrogen fixation.[23-25] While due to the lack of nitrogen active sites in TiO_2 , modification methods such as doping and construction of heterojunctions are generally required to improve the application of TiO_2 in photocatalytic nitrogen fixation.[26-28] Inspired by the structure of nitrogenase in nature, Mo element plays a key role in Fe-Mo protease. Fe-Mo nitrogenase contains Fe-Mo clusters to form bimetallic cofactors, in which Mo plays a key role.[1] Mo-based materials have been verified by theoretical calculations that have the ability to activate the triple bond of $\text{N}\equiv\text{N}$. Hexagonal molybdenum carbide (Mo_2C) is widely used in the field of photoelectric catalysis due to its good electrical conductivity and hydrogen evolution ability.[29-33] Therefore, in this work, to utilizing various virtues of Mo_2C and TiO_2 as photocatalysts, a composite material by using Mo_2C and TiO_2 for photocatalytic nitrogen fixation was designed and synthesized. Compared with pure TiO_2 , the Ti/Mo photocatalyst can effectively separate the photogenerated electrons and holes, so that this photocatalyst can convert nitrogen into ammonia efficiently from air directly.

2. Experiment

2.1 Chemicals and materials

Molybdenum acetylacetonate and glucose were purchased from Adamas-beta Reagent Co., Ltd. Nano- TiO_2 and sodium chloride (NaCl) were purchased from Shanghai Hushi Laboratorial Equipment Co., Ltd. N,N-dimethylformamide and absolute ethanol were purchased from

Sinopharm Chemical Reagent Co., Ltd. All the purchased materials have been used as analytical reagents without further purification. Deionized water was used in all the experiments.

2.2 Synthesis of Catalyst

2.2.1 Synthesis of Mo₂C@C

Mo₂C@C was prepared based on the literature with minor modifications.[31] 0.4 g molybdenum acetylacetonate and 0.14 g glucose were added in a mixture of ethanol/deionized water (5 mL, 4:1). After stirred at 70 °C for 15 minutes, 0.1 g of NaCl was added and stirred for another 10 minutes. The solution was then put into an alumina combustion boat to evaporate. The dried powder was put in a tube furnace with ventilate argon for 30 minutes to remove air. After that, the temperature of the furnace was increased to 800 °C with the rate of 5 °C/min, and kept at 800 °C for 2 hours before it naturally cooled down to room temperature. The burned black powders were washed with deionized water several times, followed by centrifugation, and dried in a vacuum oven at 90 °C to obtain a black solid Mo₂C@C. For simplicity, Mo₂C@C is named as MC in this work.

2.2.2 Synthesis of Ti/Mo

The grinded MC powder was mixed with nano-TiO₂ particles with different mass ratios (10 mg, 1:9, 2:8, 3:7, and 4:6) which was added in 10 mL absolute ethanol. Subsequently, the mixture was oscillated by an ultrasonic dispersion for 30 minutes and evaporated to obtain the solid powders. The products are denoted as TMC1, TMC2, TMC3, TMC4, corresponding to the MC mass ratio in the solid powders (10 %, 20 %, 30% and 40 %), respectively.

2.3 Characterization of the photocatalyst

The crystal phase of the sample was tested by X-ray diffractometer (XRD, Bruker AXS D8). The transmission electron microscopy (TEM, FEI Tecnai G2 F20), the scanning electron microscopy (SEM, Zeiss Sigma500) and energy-dispersive spectroscopy (EDS) were used to analyze the lattice spacing, microscopic morphology and element composition of the sample. The Raman spectrum of the sample was measured by the Raman spectrometer (Senterra II). The elemental composition of the sample was characterized by X-ray photoelectron spectroscopy (XPS, Thermo Scientific K-Alpha). The absorption spectrum was characterized by the UV-visible spectrophotometer (Hitachi U-3900). The fluorescence intensity was characterized by the fluorescence spectrophotometer, and electron spin resonance (ESR) signals were recorded with a Bruker A200 spectrometer.

The photoelectrochemical test (PEC) was performed on the CHI660E electrochemical workstation (Shanghai Chenhua, China) with a standard three-electrode configuration. The Pt plate was used as the logarithmic electrode, and Ag/AgCl was used as the reference electrode. The electrolyte was an aqueous solution of 0.5 M sodium sulfate. The photocurrent response along with time, the $I-t$ curve, was measured when a 300W xenon lamp (PLS-SXE300, Beijing Perfect Lamp Co., Ltd.) was used as the light source for intermittent lighting (20 s).

2.4 Photocatalytic nitrogen fixation test

The photocatalytic nitrogen fixation experiment was carried out in air at room temperature and normal pressure. Firstly, 5 mg of the catalyst was put into 30 mL of deionized water in the reactor. Then, the mixtures were continuously stirred (700 r/min) in the dark and bubbled with air (80

mL/min) for 30 min, before being exposed to light irradiation. 1 mL initial liquid was taken as the sample to reference. During the reaction, the reactor was irradiated with a 300W xenon lamp (PLS-SXE300, Beijing Perfect Lamp Co., Ltd.), and 1 mL of the reaction solution was collected every hour. The collected solution was filtered with a 0.22 μm filter to remove the catalyst and was detected by the indophenol blue spectrophotometry at 697.5 nm to determine the concentration of NH_3 (as NH_4^+).

2.5 $^{15}\text{N}_2$ isotope labelling experimentst

$^{15}\text{N}_2$ was used instead of air for photocatalytic nitrogen fixation experiments. The reaction solution was filtered with a 0.2 μm filter head, added sulfuric acid to evaporate and concentrated, and added deuterated DMSO-d₆ solvent for nuclear magnetic resonance test.

3. Results and discussion

3.1 Morphology and structure

In order to explore the possible crystal forms of molybdenum carbide, the samples were characterized by XRD. Figure 1 shows the XRD patterns of MC, TMC1, TMC2, TMC3 and TMC4. It can be seen that the broad diffraction peaks of MC at 39.4°, 34.4°, and 61.5° correspond to Mo_2C (PDF No. 35-0787). The TMC1, TMC2, TMC3 and TMC4 samples show a broad diffraction peak at 25.3° corresponding to anatase TiO_2 (PDF No. 21-1272), and a peak at 27.4° corresponding to rutile TiO_2 (PDF No. 21-1276). With the increase of MC, the diffraction peak of Mo_2C at 39.4° becomes more obvious, and the diffraction peak of TiO_2 is weakened. The XRD patterns indicate that TiO_2 and MC were effectively combined to obtain Ti/Mo photocatalyst by ultrasonic method.

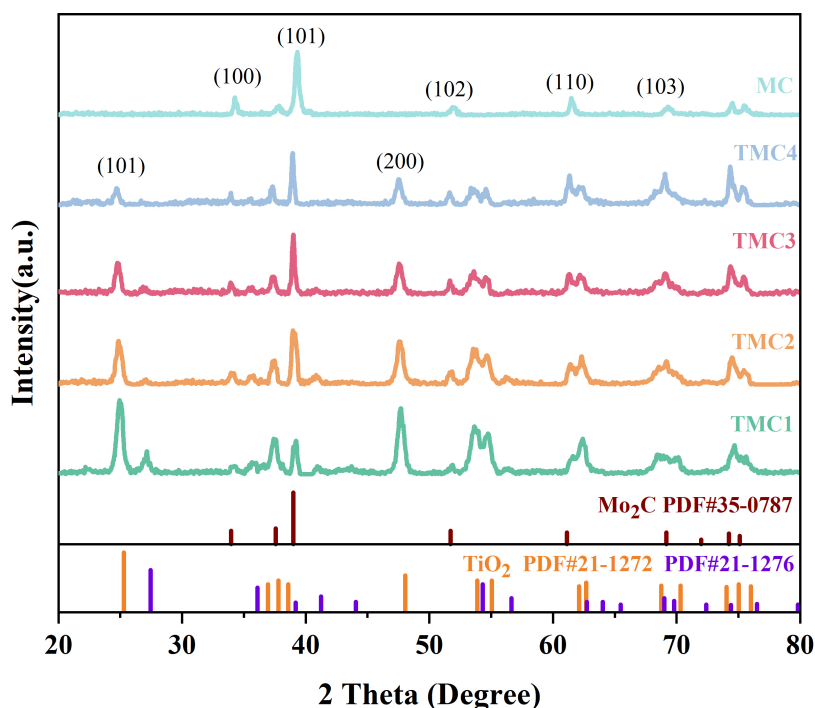


Figure. 1. XRD patterns of pure MC, TMC1, TMC2, TMC3, TMC4 samples.

More characterization of MC and TMC3 were performed, and Figure 2a are the HRTEM images of TMC3. TiO_2 can also be observed adhering to the surface in the dark. At the same time, it can be found that the interplanar lattice spacing of 0.352 nm and 0.175 nm corresponding to the (101) plane of Mo_2C and the (101) plane of TiO_2 respectively.[34, 35] In the selected area electronic diffraction (SAED) image (Figure 2b), the diffraction rings (103) and (101) correspond to the TiO_2 crystal planes, and (102) (103) (104) correspond to the Mo_2C crystal planes. These crystal planes are consistent with the XRD results, which proves the successful synthesis of TMC3.

The micromorphological features of the samples were observed by SEM. Figure 2c shows the SEM image of MC at a scale of $2\mu\text{m}$. It is observed that the pure MC has a hexagonal structure, which is consistent with previous literature.[36] Figure 2d shows the image of TMC3 after ultrasonic composite treatment. It is inferred that TiO_2 is attached to the surface of MC. Also, the elemental

mapping images of TMC3 in Figure 2 (e including e_1 to e_5) demonstrate almost overlapping distribution of Ti, O, Mo and C elements.

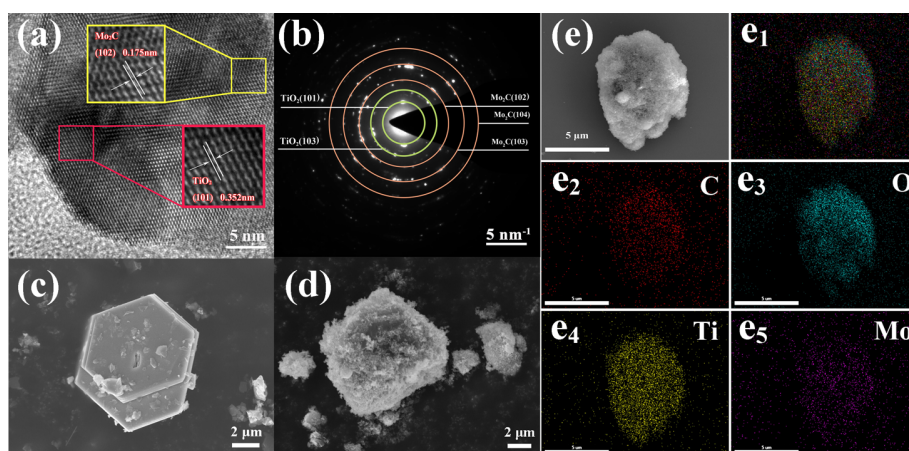


Figure. 2(a) HRTEM image of TMC3; (b) SAED image of TMC3; (c,d) SEM images of MC, TMC3; (e) the elemental mapping image of

Ti, O, Mo, C in the TMC3.

To confirm the carbon skeleton in the TMC_x samples, the samples were subjected to Raman spectroscopy. The Raman spectrum of the sample is shown in Figure 3a. The D and G bands of carbon at 1333 cm^{-1} and 1600 cm^{-1} in MC without TiO_2 indicate that glucose is converted to a carbon skeleton during the preparation process, [36, 37] and the Raman spectrum does not show the characteristic peaks of Mo_2C at 228.9 cm^{-1} and 232 cm^{-1} . The carbon peak covers the peak of Mo_2C so that the characteristic peak of Mo_2C cannot be displayed, indicating that the sample has a high graphitization. Figure 3a clearly exhibits four characteristic peaks of TiO_2 in TMC1 and TMC2 at 147 cm^{-1} , 200 cm^{-1} , 448 cm^{-1} , 400 cm^{-1} , 519 cm^{-1} , and 640 cm^{-1} . Meanwhile, the characteristic peaks of TiO_2 become stronger and the carbon peaks become less significant with the increase of TiO_2 , which means that TiO_2 can be well compounded on the surface of $\text{Mo}_2\text{C}@C$.

The chemical state and coordination environment of surface elements were investigated by XPS spectroscopy. It can be seen from Figure 3b, most of the elements in MC are carbon and

molybdenum. A small amount of oxygen may come from molybdenum oxide due to the oxidation of the sample. It is confirmed again that TMC1 and TMC2 contain four elements Ti, Mo, O, and C, which is consistent with the result of the EDS spectrum. The high-resolution spectrum of the sample TMC3 is shown in Figure 3c-f. In Figure 3c, apart from C-C at 284.7 eV and C=C at 285.4 eV, C-Mo at 283.1 eV can also be found, which is consistent with the literature. [38] Figure 3d shows the Ti-O and O-H peaks of TiO₂ at 529.7 eV and 530.3 eV, respectively. The Ti 2p XPS spectrum in Figure 3e shows two main peaks at 458.4 eV and 464.3 eV which attribute to Ti 2p_{3/2} and Ti 2p_{1/2}, respectively. Also, it can be seen that a small amount of Ti³⁺ exists, which is caused by the crystal lattice defects of TiO₂ itself.[39] From the XPS spectrum of Mo 3d (Figure 3f), the binding energy of 227.8 eV and 230.9 eV are attributable to Mo²⁺, 228.4 eV and 232.3 eV to Mo⁴⁺, and 231.7 eV and 235.2 eV to Mo⁶⁺. [40, 41] Divalent molybdenum exists in the form of Mo₂C, and the presence of tetravalent and hexavalent molybdenum may be caused by the oxidation of the sample.

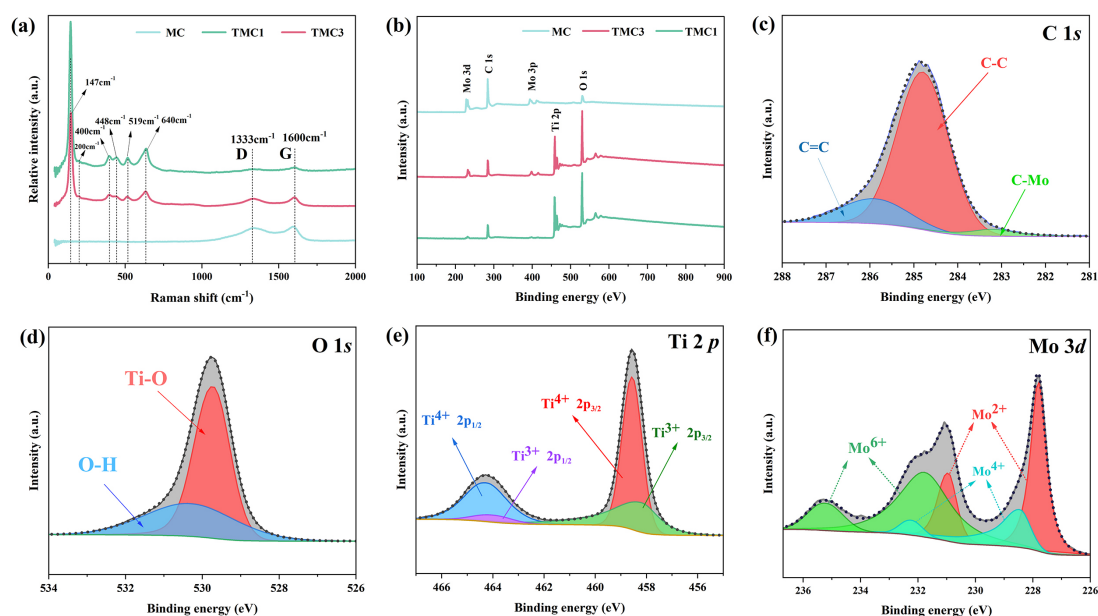


Figure 3. (a) Raman spectra of various MC, TMC1, TMC3; (b) XPS full scan spectra of MC, TMC1, TMC3; (c-f) High-resolution O 1s,

C 1s, Ti 2p, Mo 3d spectra of TMC3.

3.2 Optical Properties and Surface Features

The absorption performance of all the samples was characterized by using ultraviolet-visible diffuse reflectance spectroscopy (UV-vis). As shown in Figure 4a, the absorption peak of pure TiO₂ is at 400 nm, and MC samples loaded with different proportions show absorption bands similar to TiO₂. It shows that MC as a co-catalyst support will not affect the absorption band of TiO₂. According to previous reports,[42, 43] the Kubelka-Munk function can reflect the change of band gap energy (E_g), which can be calculated by the following equation:

$$\alpha h\nu = k(h\nu - E_g)^{n/2} \quad (1)$$

In the above equation, α is the absorption coefficient, h is the Planck constant, ν is the optical frequency, k is a constant, and the band gap energy is expressed by E_g . Since TiO₂ is an indirect semiconductor which band gap n is 4. As shown in the Figure 4a, the calculated band gap energy (E_g) of the sample TMC_x ($x = 1, 2, 3, 4$) and TiO₂ are 3.01, 3.04, 3.03, 2.98, 2.98 eV, respectively.[44, 45]

Photoluminescence (PL) spectra can be employed to determine the recombination rate of photogenerated electron-hole pairs. In general, the stronger the fluorescence, the higher the recombination rate of photogenerated electrons and holes in the sample. As shown in Figure 4b, all samples fluoresce at 724 nm. The highest fluorescence intensity is produced by pure TiO₂. The fluorescence effect is obviously weakened when MC is loaded. Sample TMC3 exhibits the weakest fluorescence, indicating that this sample has the lowest recombination rate of photogenerated electrons and holes.

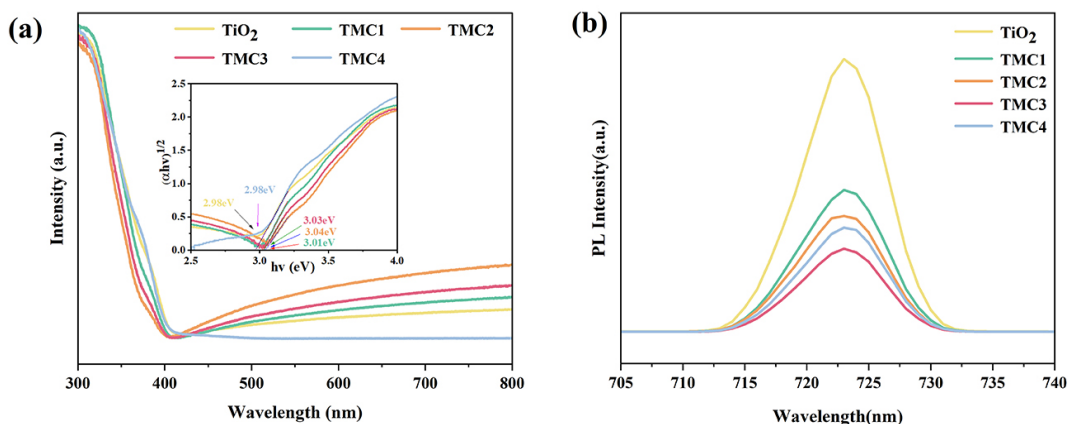


Figure 4. UV-vis absorption spectra profiles; (b) PL spectra of pure TiO₂, TMC1, TMC2, TMC3, and TMC4.

To study the adsorption behavior of sample TMC3 to nitrogen, the sample was subjected to nitrogen adsorption analysis and specific surface area test. As shown in Figure 5a, the adsorbed nitrogen volume of pure TiO₂ is higher than TMC3, indicating TMC3 has a larger specific surface area. The specific surface area of pure TiO₂ and TMC3 was obtained by the BET method, notably the specific area of TMC3 is 562.53 m²/g, which is much higher than that of pure TiO₂ (53.48 m²/g). Therefore, Mo₂C@C has a larger specific surface area, which can absorb more N₂ and facilitate the reaction. Figure 5b shows the electron paramagnetic resonance (ESR) test diagram of sample TMC3 and TiO₂. Sample TMC3 has an obvious peak at $g = 2.001$ [46-48], and pure TiO₂ has no obvious signal peak. This may be due to the carbon vacancy defects caused by the deletion of carbon atoms during the formation of Mo₂C by argon high-temperature sintering. And the lack of some carbon atoms provides active sites for the conversion of nitrogen to ammonia.[49, 50] The defect signal peak is almost undetectable for pure TiO₂, while TMC3 has an obvious signal peak. This may be due to the lattice defects caused by high-temperature sintering of inert gases in accordance with the result in Figure 5b, since it is known that the generation of lattice defects provides active sites for

the conversion of nitrogen to ammonia.

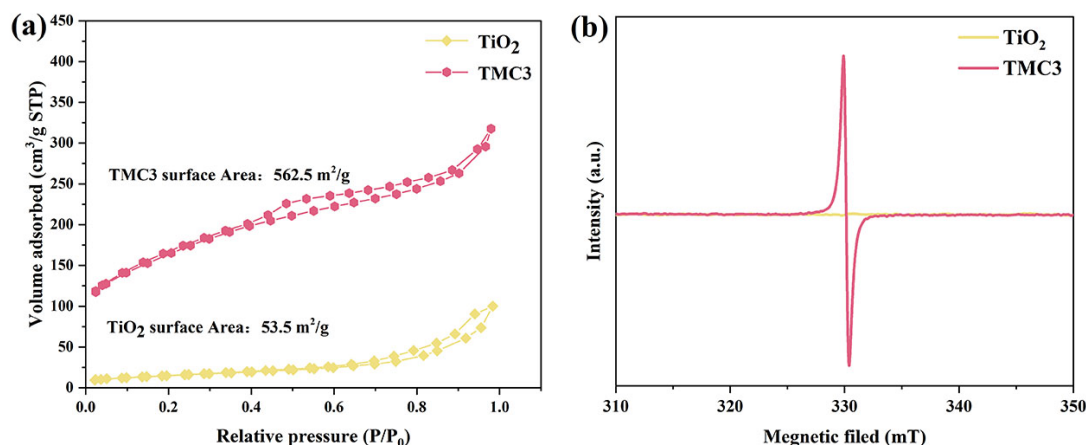


Figure 5. (a) BET adsorption-desorption isotherms of pure TiO_2 and TMC3; (b) ESR spectra of pure TiO_2 and TMC3.

The EIS measurements were performed on pure TiO_2 and TMC_x ($x=1,2,3,4$) to measure the internal resistance for the charge transfer process. As shown in Figure 6a, the sample TMC3 impedance radius is the smallest among all samples. The smaller the radius is, the easier the electron transmission can happen. The loaded TiO_2 on MC can transmit photo-generated electrons to Mo_2C and increase the transmission rate of photo-generated electrons. At the same time, the photo-generated current process of the samples of pure TiO_2 and TMC3 was studied. The transient photocurrent response can directly reflect the life-time of photo-generated charge carriers and the separation efficiency of electron-hole pairs when the xenon lamp is repeatedly switched on and off for 20 seconds. As shown in Figure 6b, the TMC3 photocurrent density of $1.5 \mu\text{A}/\text{cm}^2$ is higher than the pure TiO_2 photocurrent density of $1.0 \mu\text{A}/\text{cm}^2$, indicating that the sample TMC3 has a higher photogenerated charge carrier density. The decrease in impedance and the increase in photocurrent are beneficial to converting nitrogen to ammonia.

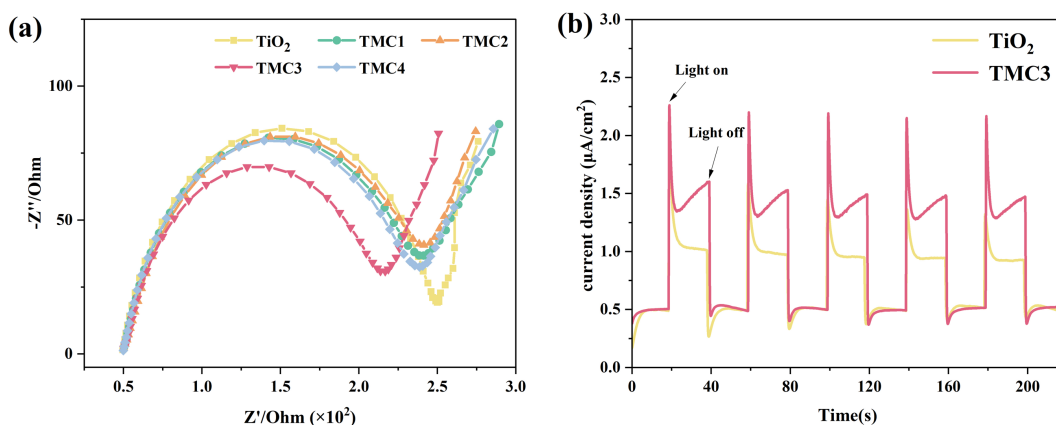


Figure 6. (a) EIS Nyquist plots of pure TiO_2 and $\text{TMC}_x(x=1,2,3,4)$; (b) Transient photocurrent responses of pure TiO_2 and TMC_3 .

3.3 Photocatalytic nitrogen fixation performance and mechanism

3.3.1 Nitrogen fixation performance of TMC_x photocatalyst

In the photocatalytic nitrogen fixation experiment, the catalyst was irradiated by ultraviolet light in an aqueous solution under high-purity nitrogen atmosphere to evaluate the photocatalytic nitrogen fixation performance of all samples. As shown in Figure 7a, the time growth rate of NH_4^+ is relatively stable, and the content of NH_4^+ continues to increase with time. The growth rate of NH_4^+ of TMC_3 sample is about $432 \mu\text{g} \cdot \text{g}_{\text{cat}}^{-1} \cdot \text{h}^{-1}$, which is 16 times that of pure TiO_2 . The ammonium radical detection method adopts indophenol blue spectrophotometry to detect at 697.5 nm. Sample TMC_3 was subjected to simulated sunlight-catalytic nitrogen fixation experiments under a xenon lamp (300 w) with a solar filter (Figure 7b). The ammonia production efficiency was about $353 \mu\text{g} \cdot \text{g}_{\text{cat}}^{-1} \cdot \text{h}^{-1}$. When the TMC_3 sample was test in Ar atmosphere or without light (Figure 7b), it can be seen that the generation of ammonium needs to be carried out under light with nitrogen as the required raw material. The stability performance was also examined. The apparent quantum efficiency (AQE = 0.1%) of sample TMC_3 was obtained by the nitrogen fixation experiment with a single-band 365 nm light source, the calculation formula based on literature [1] is as follows:

$$\text{AQE (\%)} = \frac{N_e}{N_p} \times 100\% = \frac{3 \times \text{The number of molecules of NH}_3 \text{ produced}}{\text{The number of incident photons}} \times 100\% \quad (2)$$

It can be seen from Figure 7c that the catalytic performance of the catalyst remains basically stable in 5 cycles per 5 h, and the XRD patterns (Figure S3) basically unchanged after the reaction, indicating that the sample is stable. The ^{15}N isotope N_2 labelling method proved the reliability of the conversion of N_2 to ammonia (Figure S4). Substituting $^{15}\text{N}_2$ for $^{14}\text{N}_2$ in photocatalytic nitrogen fixation reaction, then acidifying the reaction solution, $^{15}\text{NH}_4^+$ was detected by nuclear magnetism. This result shows that the nitrogen source comes from the external nitrogen atmosphere directly.

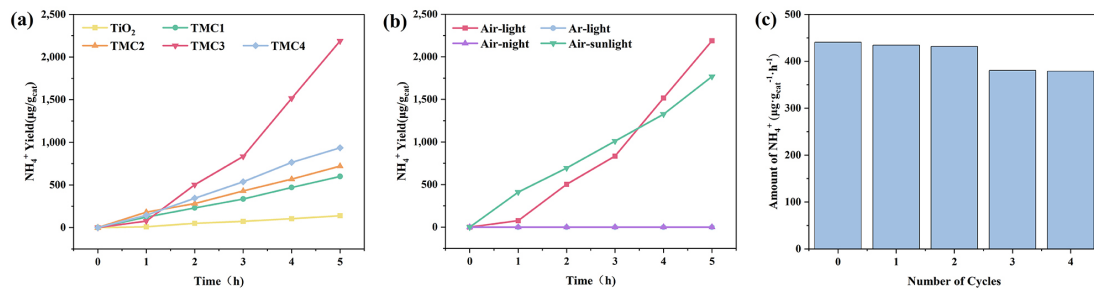


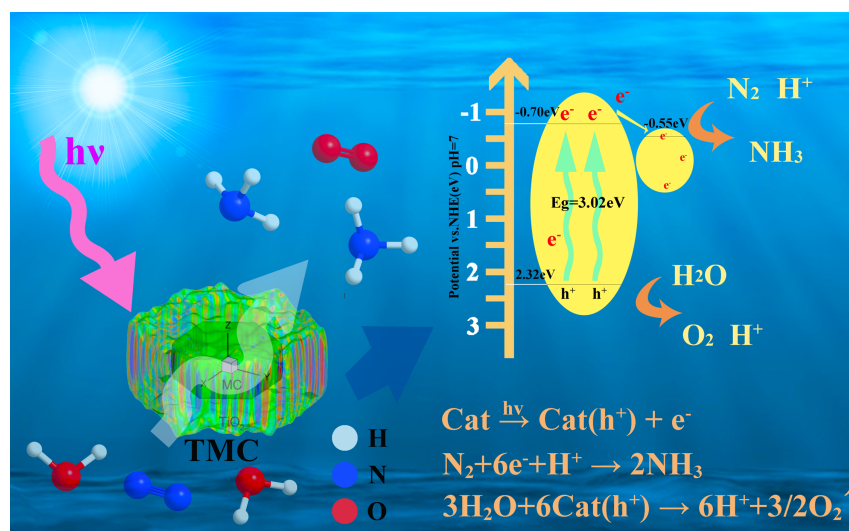
Figure 7. (a) Quantitative determination of the generated NH_3 under UV light; (b) Photocatalytic nitrogen fixation tests for TMC3 under different conditions; (c) Catalyst cycling tests for TMC3.

3.3.2 Photocatalytic nitrogen fixation mechanism

In order to obtain the conduction band potential of TiO_2 and MC, the Mott-Schottky plots of the sample TiO_2 and MC were obtained through the electrochemical test. As shown in Figure S5a, b, the $1/C^2$ to potential curves are obliquely cut to the X axis, and the intersection points are the flat band potentials (E_{fb}) of sample TiO_2 and MC, which are -0.60 eV and -0.45 eV, respectively. The conduction band potential (E_{cb}) is estimated by subtracting 0.1 eV from E_{fb} , so the E_{cb} of sample TiO_2 is -0.70 eV, which is more negative than that of sample MC ($E_{\text{cb}} = -0.55$ eV). The forbidden band width (E_{g}) of TiO_2 is 3.02 eV which is calculated by solid ultraviolet diffuse reflectance spectrum (Figure 4.a). The valence band potential of TiO_2 is calculated to be 2.32 eV by the formula

$E_{vb} = E_g + E_{cb}$. It has been reported that the reduction potential when N_2 is converted to NH_3 is $-0.092V$ vs. NHE. The oxidation potential of H_2O to O_2 is $+1.23V$ vs. NHE.[51 52]

Based on the above analysis and previous studies [53], a hypothetical mechanism for photocatalytic nitrogen reduction electron transfer was proposed. In the heterojunction formed by TiO_2 and MC, the conduction band potential of Mo_2C satisfies the conversion of N_2 to NH_3 and is lower than the conduction band potential of TiO_2 , so that photoelectrons can be transferred from TiO_2 to Mo_2C . The sample MC prepared in this study has a highly graphitized carbon layer structure (shown in Figure 3.a), and the photoelectrons are easily concentrated on Mo_2C due to the excellent electrical conductivity of the carbon layer. Nitrogen is easily adsorbed at the carbon vacancies of the molybdenum atoms to receive photoelectrons, and the activated nitrogen is combined with the protons in water and finally reduced to ammonia. Hydroxyl radicals generated by photocatalytic water splitting of the catalyst were detected in the ESR free radical test (Figure S2.b), confirming the water splitting process. It is inferred from the hydroxyl radical test that the water molecules adsorbed on the surface of TiO_2 are oxidized by TiO_2 holes and eventually form O_2 . The following equations related to the reaction are summarized in Scheme 1.



Scheme 1. Schematic illustration showing the mechanism for photocatalytic nitrogen fixation.

3.4 Interactions between light and TMCx photocatalytic particle

Numerical simulations via the field-only surface integral method [54-58] were also carried out to study the interactions between light and the synthesized TMCx photocatalytic particles to further confirm that TMCx can be an effective and efficient material for photocatalyst. The focus of the calculation is the absorption cross section of a TMCx photocatalytic particle which represents how much energy from the sunlight can be utilized by such a particle.

Figure 2c and 2d indicate that the TMCx particle should be with a core-shell structure as MC@TiO₂ in which the MC core is a thin regular hexagon and the TiO₂ is a hexagon with some surface roughness. The typical edge length of the hexagonal MC particle is 2 μm and the thickness was set as 120 nm. The aspect ratio of the TiO₂ shell is the same as the MC core, and for the TMC3 particle, the edge length of the TiO₂ shell is 1.8 times of the MC core given the densities of and mass ratio between TiO₂ and MC. The irregular surface roughness on TiO₂ was represented by the Gaussian random particle.

The sunlight is represented by a spectrum of plane electromagnetic waves with time dependence of $\exp(-i\omega t)$ where ω is the angular frequency of the light and i is the imaginary unit. We screened the wavelength spectrum of sunlight λ from 300 nm to 800 nm with a step of 20 nm. The illumination plane wave propagates perpendicular to the thin TMC particle (along z -direction) as $\mathbf{k}^{\text{inc}} = (0, 0, k_0)$ with $k_0 = 2\pi/\lambda$ being the wavenumber, and its electric field polarizes along x -direction as $\mathbf{E}^{\text{inc}} = \mathbf{E}_0 \exp(ik_0 z)$ with $\mathbf{E}_0 = (E_0, 0, 0)$ (see Figure 8a). The scattered electromagnetic fields in the solution, \mathbf{E}^{sca} and \mathbf{H}^{sca} , and the transmitted fields within the core-shell particle were calculated following the idea in the literature.[57,59] The refractive index of the solution (water) was set as $n_{\text{water}} = 1.33$. The refractive index n_{MC} and extinction

coefficient k_{MC} of MC were calculated by using the first- principles simulations,[60] and the refractive index n_{TiO_2} and extinction coefficient k_{TiO_2} of the traditional photocatalyst material TiO_2 can be found in the literature.[61]

Figure 8a displays the distribution of the surface charge density, $q = \mathbf{E} \cdot \mathbf{n}$, on both surfaces of the MC@ core-shell particle when $\lambda = 540$ nm. Figure 8b presents the variation of absorption cross section $\sigma^{abs} = \int_S \frac{1}{2} \text{Real}[\mathbf{E}^{tot} \times (\mathbf{H}^{tot})^*] dS$ along the wavelengths of sunlight where $\mathbf{E}^{tot} = \mathbf{E}^{inc} + \mathbf{E}^{sca}$ and $\mathbf{H}^{tot} = \mathbf{H}^{inc} + \mathbf{H}^{sca}$, superscript * indicates the conjugate of the field values, and S is a surface that encloses the particle. Obvious absorption of sunlight indicates that TMC is an effective photocatalyst material to harvest solar energy. Also, the trend of σ^{abs} across the sunlight spectrum from the simulation in Figure 8b is in good agreement relative to the absorption measured in the experiments as shown in Figure 4a, which means that the assumed core-shell structure of the TMC particle in the simulations is valid.

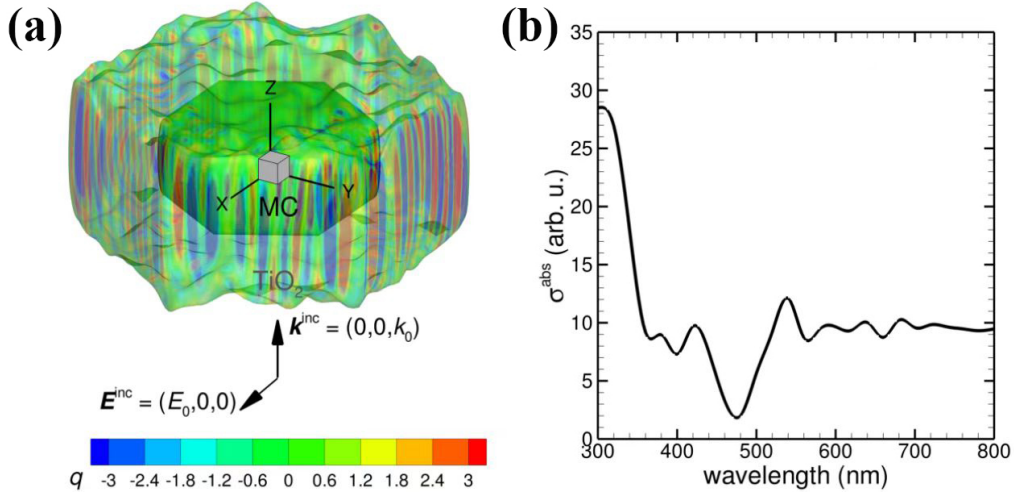


Figure 8. (a) Sketch and surface charge distribution, q , of a TMC particle with MC@ TiO_2 core-shell structure under the illumination of sunlight (Note the length scale in the z -direction is 13 times of that in the xy -plane for good visualization). (b) Absorption cross sections

of a TMC particle across the spectrum of sunlight.

4. Conclusion

In summary, a carbon-coated hexagonal Ti/Mo photocatalyst for nitrogen fixation from air directly has been developed. Nitrogen is converted to ammonia under 300W xenon lamp at room temperature and normal pressure, and the reliability of N₂ reduction to ammonia has been proved by ¹⁵N₂ isotope labelling. The highest NH₃ generation rate of sample TMC3 is achieved to be 432 μg·g_{cat}⁻¹·h⁻¹, which is 16 times higher than that of pure TiO₂. The field-only surface integral method were performed to confirm that it can be an efficient photocatalyst. This study provides a pathway for the feasibility of utilizing Mo₂C in the combination with traditional photocatalyst TiO₂ for photocatalytic nitrogen fixation.

Acknowledgement

We are thankful to the National Natural Science Foundation of China (21978061) and Zhejiang Key Laboratory of Green Pesticides and Cleaner Production Technology for providing financial support. Q. Sun acknowledges the support by the Australian Research Council (ARC) through grants DE150100169, FT160100357 and CE140100003. This research was undertaken with the assistance of resources from the National Computational Infrastructure (NCI Australia), an NCRIS enabled capability supported by the Australian Government.

References

- [1] K. An, H.J. Ren, D. Yang, Z.F. Zhao, Y.C. Gao, Y. Chen, J.D. Tan, W.J. Wang, Z.Y. Jiang, Nitrogenase-inspired bimetallic metal organic frameworks for visible-light-driven nitrogen fixation, *Appl. Catal., B* 292 (2021) 120167. <https://doi.org/10.1016/j.apcatb.2021.120167>.

- [2] L. Zhang, M. Cong, X. Ding, Y. Jin, F. Xu, Y. Wang, L. Chen, L. Zhang, A Janus Fe-SnO₂ Catalyst that Enables Bifunctional Electrochemical Nitrogen Fixation, *Angew. Chem., Int. Ed.* 59 (2020) 10888-10893. <https://doi.org/10.1002/anie.202003518>.
- [3] H. Xu, Y. Wang, X. Dong, N. Zheng, H. Ma, X. Zhang, Fabrication of IN₂O₃/IN₂S₃ microsphere heterostructures for efficient and stable photocatalytic nitrogen fixation, *Appl. Catal., B* 257 (2019) 117932. <https://doi.org/10.1016/j.apcatb.2019.117932>.
- [4] S. Zhang, Y. Zhao, R. Shi, C. Zhou, G.I.N. Waterhouse, Z. Wang, Y. Weng, T. Zhang, Sub-3 nm Ultrafine Cu₂O for Visible Light Driven Nitrogen Fixation, *Angew. Chem., Int. Ed.* 60 (2021) 2554-2560. <https://doi.org/10.1002/anie.202013594>.
- [5] G. Zhang, C.D. Sewell, P. Zhang, H. Mi, Z. Lin, Nanostructured photocatalysts for nitrogen fixation, *Nano Energy* 71 (2020) 104645. <https://doi.org/10.1016/j.nanoen.2020.104645>.
- [6] Y. Shen, L. Chen, L. Zhang, W. Han, M. Jiang, H. Zheng, Nitrogen fixation from air at normal temperature and pressure via Cobalt-iron photocatalyst day and night, *Mol. Catal.* 518 (2022) 112091. <https://doi.org/10.1016/j.mcat.2021.112091>.
- [7] A. Klerke, C.H. Christensen, J.K. Nørskov, T. Vegge, AmMonia for hydrogen storage: challenges and opportunities, *J. Mater. Chem.* 18 (2008) 2304. <https://doi.org/10.1039/b720020j>.
- [8] H. Huang, X.-S. Wang, D. Philo, F. Ichihara, H. Song, Y. Li, D. Li, T. Qiu, S. Wang, J. Ye, Toward visible-light-assisted photocatalytic nitrogen fixation: A titanium metal organic framework with functionalized ligands, *Appl. Catal., B* 267 (2020) 118686. <https://doi.org/10.1016/j.apcatb.2020.118686>.

- [9] P. Qiu, C. Huang, G. Dong, F. Chen, F. Zhao, Y. Yu, X. Liu, Z. Li, Y. Wang, Plasmonic gold nanocrystals simulated efficient photocatalytic nitrogen fixation over Mo doped W18O49 nanowires, *J. Mater. Chem. A* 9 (2021) 14459-14465. <https://doi.org/10.1039/d1ta03339e>.
- [10] M. Que, Y. Zhao, Y. Yang, L. Pan, W. Lei, W. Cai, H. Yuan, J. Chen, G. Zhu, Anchoring of Formamidinium Lead Bromide Quantum Dots on Ti3C2 Nanosheets for Efficient Photocatalytic Reduction of CO₂, *ACS. Appl. Mater. Interfaces*. 13 (2021) 6180-6187. <https://doi.org/10.1021/acscami.0c18391>.
- [11] J. Li, P. Liu, Y. Tang, H. Huang, H. Cui, D. Mei, C. Zhong, Single-Atom Pt-N₃ Sites on the Stable Covalent Triazine Framework Nanosheets for Photocatalytic N₂ Fixation, *ACS Catal.*10 (2020) 2431-2442. <https://doi.org/10.1021/acscatal.9b04925>.
- [12] J. Di, J. Xia, M.F. Chisholm, J. Zhong, C. Chen, X. Cao, F. Dong, Z. Chi, H. Chen, Y.X. Weng, J. Xiong, S.Z. Yang, H. Li, Z. Liu, S. Dai, Defect-Tailoring Mediated Electron-Hole Separation in Single-Unit-Cell Bi₃O₄ Br Nanosheets for Boosting Photocatalytic Hydrogen Evolution and Nitrogen Fixation, *Adv Mater* 31 (2019) e1807576. <https://doi.org/10.1002/adma.201807576>.
- [13] S. Bian, M. Wen, J. Wang, N. Yang, P.K. Chu, X.F. Yu, Edge-Rich Black Phosphorus for Photocatalytic Nitrogen Fixation, *J. Phys. Chem. Lett.*11 (2020) 1052-1058. <https://doi.org/10.1021/acs.jpcclett.9b03507>.
- [14] H. Tao, C. Choi, L.-X. Ding, Z. Jiang, Z. Han, M. Jia, Q. Fan, Y. Gao, H. Wang, A.W. Robertson, S. Hong, Y. Jung, S. Liu, Z. Sun, Nitrogen Fixation by Ru Single-Atom Electrocatalytic Reduction, *Chem* 5 (2019) 204-214. <https://doi.org/10.1016/j.chempr.2018.10.007>.

- [15] B. Qin, Y. Li, Q. Zhang, G. Yang, H. Liang, F. Peng, Understanding of nitrogen fixation electrocatalyzed by Molybdenum–iron carbide through the experiment and theory, *Nano Energy* 68 (2020) 104374. <https://doi.org/10.1016/j.nanoen.2019.104374>.
- [16] S. Mansingh, K.K. Das, S. Sultana, K. Parida, Recent advances in wireless photofixation of dinitrogen to ammonia under the ambient condition: A review, *J. Photochem. Photobiol., C* 47 (2021) 100402. <https://doi.org/10.1016/j.jphotochemrev.2021.100402>.
- [17] L. Shi, Y. Yin, S. Wang, H. Sun, Rational Catalyst Design for N₂ Reduction under Ambient Conditions: Strategies toward Enhanced Conversion Efficiency, *ACS Catal.* 10 (2020) 6870-6899. <https://doi.org/10.1021/acscatal.0c01081>.
- [18] S.A. Younis, E.E. Kwon, M. Qasim, K.-H. Kim, T. Kim, D. Kukkar, X. Dou, I. Ali, Metal-organic framework as a photocatalyst: Progress in Modulation strategies and environmental/energy applications, *Prog. Energy Combust. Sci.* 81 (2020) 100870. <https://doi.org/10.1016/j.pecs.2020.100870>.
- [19] Q.-Y. Liu, H.-D. Wang, R. Tang, Q. Cheng, Y.-J. Yuan, Rutile TiO₂ Nanoparticles with Oxygen Vacancy for Photocatalytic Nitrogen Fixation, *ACS Appl. Nano Mater.* 4 (2021) 8674-8679. <https://doi.org/10.1021/acsanm.1c02184>.
- [20] S. Liu, S. Wang, Y. Jiang, Z. Zhao, G. Jiang, Z. Sun, Synthesis of Fe₂O₃ loaded porous g-C₃N₄ photocatalyst for photocatalytic reduction of dinitrogen to ammonia, *Chem. Eng. J.* 373 (2019) 572-579. <https://doi.org/10.1016/j.cej.2019.05.021>.
- [21] Z. He, Y. Wang, X. Dong, N. Zheng, H. Ma, X. Zhang, Indium sulfide nanotubes with sulfur vacancies as an efficient photocatalyst for nitrogen fixation, *RSC Adv.* 9 (2019) 21646-21652. <https://doi.org/10.1039/c9ra03507a>.

- [22] H. Zheng, X. Meng, J. Chen, M. Que, W. Wang, X. Liu, L. Yang, Y. Zhao, In situ phase evolution of TiO₂/Ti₃C₂T heterojunction for enhancing adsorption and photocatalytic degradation, Appl. Surf. Sci. 545 (2021). <https://doi.org/10.1016/j.apsusc.2021.149031>.
- [23] X. Bian, Y. Zhao, S. Zhang, D. Li, R. Shi, C. Zhou, L.-Z. Wu, T. Zhang, Enhancing the Supply of Activated Hydrogen to Promote Photocatalytic Nitrogen Fixation, ACS Mater. Lett. 3 (2021) 1521-1527. <https://doi.org/10.1021/acsmaterialslett.1c00504>.
- [24] T. Hou, Q. Li, Y. Zhang, W. Zhu, K. Yu, S. Wang, Q. Xu, S. Liang, L. Wang, Near-infrared light-driven photofixation of nitrogen over Ti₃C₂T_x/TiO₂ hybrid structures with superior activity and stability, Appl. Catal., B 273 (2020) 119072. <https://doi.org/10.1016/j.apcatb.2020.119072>.
- [25] A. Naldoni, M. Altomare, G. Zoppellaro, N. Liu, S. Kment, R. Zboril, P. Schmuki, Photocatalysis with Reduced TiO₂: From Black TiO₂ to Cocatalyst-Free Hydrogen Production, ACS Catal. 9 (2019) 345-364. <https://doi.org/10.1021/acscatal.8b04068>.
- [26] C. Hao, Y. Liao, Y. Wu, Y. An, J. Lin, Z. Gu, M. Jiang, S. Hu, X. Wang, RuO₂-loaded TiO₂-MXene as a high performance photocatalyst for nitrogen fixation, J. Phys. Chem. Solids 136 (2020) 109141. <https://doi.org/10.1016/j.jpcs.2019.109141>.
- [27] M. Ilkaeva, I. Krivtsov, E. Diaz, Z. Amghouz, Y. Patino, S. Khainakov, J.R. Garcia, S. Ordonez, Photocatalytic degradation of 2-(4-methylphenoxy)ethanol over TiO₂ spheres, J. Hazard. Mater. 332 (2017) 59-69. <https://doi.org/10.1016/j.jhazmat.2017.02.055>.
- [28] Y. Liu, Z. Yu, S. Guo, L. Yao, R. Sun, X. Huang, W. Zhao, Photocatalytic nitrogen fixation on transition metal Modified TiO₂ nanosheets under simulated sunlight, New J. Chem. 44 (2020) 19924-19932. <https://doi.org/10.1039/d0nj04397d>.

- [29] K. Ba, G. Wang, T. Ye, X. Wang, Y. Sun, H. Liu, A. Hu, Z. Li, Z. Sun, Single Faceted Two-Dimensional Mo₂C Electrocatalyst for Highly Efficient Nitrogen Fixation, ACS Catal. 10 (2020) 7864-7870. <https://doi.org/10.1021/acscatal.0c01127>.
- [30] H.-Q. Chang, G.-H. Zhang, K.-C. Chou, Topochemical synthesis of one-dimensional Mo₂C nanobelts, Ceram. Int. 46 (2020) 12891-12896. <https://doi.org/10.1016/j.ceramint.2020.01.224>.
- [31] H. Cheng, L.X. Ding, G.F. Chen, L. Zhang, J. Xue, H. Wang, Molybdenum Carbide Nanodots Enable Efficient Electrocatalytic Nitrogen Fixation under Ambient Conditions, Adv. Mater. 30 (2018) e1803694. <https://doi.org/10.1002/adma.201803694>.
- [32] L. Gao, J. Liu, H. Long, P. Wang, H. Yu, One-step calcination synthesis of WC–Mo₂C heterojunction nanoparticles as novel H₂-production cocatalysts for enhanced photocatalytic activity of TiO₂, Catal. Sci. Technol. 11 (2021) 7307-7315. <https://doi.org/10.1039/d1cy01581h>.
- [33] Y. Zhou, W. Wang, C. Zhang, D. Huang, C. Lai, M. Cheng, L. Qin, Y. Yang, C. Zhou, B. Li, H. Luo, D. He, Sustainable hydrogen production by Molybdenum carbide-based efficient photocatalysts: From properties to mechanism, Adv. Colloid Interface Sci. 279 (2020) 102144. <https://doi.org/10.1016/j.cis.2020.102144>.
- [34] Y. Liu, Z. Ye, D. Li, M. Wang, Y. Zhang, W. Huang, Tuning CuO_x-TiO₂ interaction and photocatalytic hydrogen production of CuO_x/TiO₂ photocatalysts via TiO₂ Morphology engineering, Appl. Surf. Sci. 473 (2019) 500-510. <https://doi.org/10.1016/j.apsusc.2018.12.177>.
- [35] H. Wang, Y. Cao, C. Sun, G. Zou, J. Huang, X. Kuai, J. Zhao, L. Gao, Strongly Coupled Molybdenum Carbide on Carbon Sheets as a Bifunctional Electrocatalyst for Overall Water Splitting, ChemSusChem 10 (2017) 3540-3546. <https://doi.org/10.1002/cssc.201701276>.

- [36] C. Xu, Q. Wang, S. Zhao, S. Wang, NiCo₂O₄ nanoneedle/Mo₂C-coated carbon cloth as efficient catalyst for water splitting and metal-air battery, *Synth. Met.* 280 (2021) 116894. <https://doi.org/10.1016/j.synthmet.2021.116894>.
- [37] H. Xin, Y. Hai, D. Li, Z. Qiu, Y. Lin, B. Yang, H. Fan, C. Zhu, Coupling Mo₂C@C core-shell nanocrystals on 3D graphene hybrid aerogel for high-performance lithium ion battery, *Appl. Surf. Sci.* 441 (2018) 69-76. <https://doi.org/10.1016/j.apsusc.2018.01.187>.
- [38] Y. Tan, M. Yi, Z. Zhu, X. Zhang, K. Qin, J. Zhang, R. Zhu, Carbon-coated MoSe₂/Mo₂CT_x (MXene) heterostructure for efficient hydrogen evolution, *Mater. Sci. Eng., B* 271 (2021) 115239. <https://doi.org/10.1016/j.mseb.2021.115239>.
- [39] J. Wang, X. Wang, Q. Chen, H. Xu, M. Dai, M. Zhang, W. Wang, H. Song, Microstructural Modification of hollow TiO₂ nanospheres and their photocatalytic performance, *Appl. Surf. Sci.* 535 (2021) 147641. <https://doi.org/10.1016/j.apsusc.2020.147641>.
- [40] F. Turker, O.R. Caylan, N. Mehmood, T.S. Kasirga, C. Sevik, G. Cambaz Buke, CVD synthesis and characterization of thin Mo₂C crystals, *J. Am. Ceram. Soc.* 103 (2020) 5586-5593. <https://doi.org/10.1111/jace.17317>.
- [41] L. Yang, W. Chen, R. Yang, A. Chen, H. Zhang, Y. Sun, Y. Jia, X. Li, Z. Tang, X. Gui, Fabrication of MoO_x/Mo₂C-Layered Hybrid Structures by Direct Thermal Oxidation of Mo₂C, *ACS Appl. Mater. Interfaces* 12 (2020) 10755-10762. <https://doi.org/10.1021/acsami.9b18650>.
- [42] G.K. Pradhan, D.K. Padhi, K.M. Parida, Fabrication of alpha-Fe₂O₃ nanorod/RGO composite: a novel hybrid photocatalyst for phenol degradation, *ACS Appl. Mater. Interfaces* 5 (2013) 9101-9110. <https://doi.org/10.1021/am402487h>.

- [43] M. Tasbihi, K. Koci, I. Troppova, M. Edelmannova, M. Reli, L. Capek, R. Schomacker, Photocatalytic reduction of carbon dioxide over Cu/TiO₂ photocatalysts, *Environ. Sci. Pollut. Res. Int.* 25 (2018) 34903-34911. <https://doi.org/10.1007/s11356-017-0944-8>.
- [44] H. She, X. Ma, K. Chen, H. Liu, J. Huang, L. Wang, Q. Wang, Photocatalytic H₂ production activity of TiO₂ Modified by inexpensive Cu(OH)₂ cocatalyst, *J. Alloys Compd.* 821 (2020) 153239. <https://doi.org/10.1016/j.jallcom.2019.153239>.
- [45] Z. Qin, L. Chen, R. Ma, R. ToMovska, X. Luo, X. Xie, T. Su, H. Ji, TiO₂/BiYO₃ composites for enhanced photocatalytic hydrogen production, *J. Alloys Compd.* 836 (2020) 155428. <https://doi.org/10.1016/j.jallcom.2020.155428>.
- [46] P. Zhang, L.-J. Wu, W.-G. Pan, Z.-Z. Wei, X.-Y. Liang, R.-T. Guo, Granular Polymeric Carbon Nitride with Carbon Vacancies for Enhanced Photocatalytic Hydrogen Evolution, *Sol. RRL* 5 (2021) 2000796. <https://doi.org/10.1002/solr.202000796>.
- [47] M. Liu, D. Zhang, J. Han, C. Liu, Y. Ding, Z. Wang, A. Wang, Adsorption enhanced photocatalytic degradation sulfadiazine antibiotic using porous carbon nitride nanosheets with carbon vacancies, *Chem. Eng. J.* 382 (2020) 123017. <https://doi.org/10.1016/j.cej.2019.123017>.
- [48] M. Shen, L. Zhang, M. Wang, J. Tian, X. Jin, L. Guo, L. Wang, J. Shi, Carbon-vacancy Modified graphitic carbon nitride: enhanced CO₂ photocatalytic reduction performance and mechanism probing, *J. Mater. Chem. A* 7 (2019) 1556-1563. <https://doi.org/10.1039/c8ta09302d>.
- [49] Y. Zhang, J. Di, P. Ding, J. Zhao, K. Gu, X. Chen, C. Yan, S. Yin, J. Xia, H. Li, Ultrathin g-C₃N₄ with enriched surface carbon vacancies enables highly efficient photocatalytic nitrogen fixation, *J. Colloid Interface Sci.* 553 (2019) 530-539. <https://doi.org/10.1016/j.jcis.2019.06.012>.

- [50] M. Cheng, C. Xiao, Y. Xie, Photocatalytic nitrogen fixation: the role of defects in photocatalysts, *J. Mater. Chem. A* 7 (2019) 19616-19633. <https://doi.org/10.1039/c9ta06435d>.
- [51] M.H. Vu, M. Sakar, S.A. Hassanzadeh - Tabrizi, T.O. Do, Photo(electro)catalytic Nitrogen Fixation: Problems and Possibilities, *Adv. Mater. Interfaces* 6 (2019) 1900091. <https://doi.org/10.1002/admi.201900091>.
- [52] E. Vesali-Kermani, A. Habibi-Yangjeh, H. Diarmand-Khalilabad, S. Ghosh, Nitrogen photofixation ability of g-C₃N₄ nanosheets/Bi₂MoO₆ heterojunction photocatalyst under visible-light illumination, *J. Colloid Interface Sci.* 563 (2020) 81-91. <https://doi.org/10.1016/j.jcis.2019.12.057>.
- [53] J. Liu, P. Wang, J. Fan, H. Yu, Carbon-coated cubic-phase molybdenum carbide nanoparticle for enhanced photocatalytic H₂-evolution performance of TiO₂. *J. Energy Chem.* (51) 2020 253-261. <https://doi.org/10.1016/j.jechem.2020.03.085>.
- [54] E. Klaseboer, Q. Sun, D.Y.C. Chan, Nonsingular Field-Only Surface Integral Equations for Electromagnetic Scattering, *IEEE Trans. Antennas Propag.* 65 (2017) 972-977. <https://doi.org/10.1109/tap.2016.2632619>.
- [55] Q. Sun, E. Klaseboer, D.Y.C. Chan, Robust multiscale field-only formulation of electromagnetic scattering, *Phys. Rev. B* 95 (2017). <https://doi.org/10.1103/PhysRevB.95.045137>.
- [56] Q. Sun, E. Klaseboer, A. J. Yuffa, D. Y. C. Chan, Field-only surface integral equations: scattering from a perfect electric conductor, *J. Opt. Soc. Am. A* 37 (2020) 276-283. <https://doi.org/10.1364/josaa.378665>.
- [57] Q. Sun, E. Klaseboer, A. J. Yuffa, D. Y. C. Chan, Field-only surface integral equations: scattering from a dielectric body. *J. Opt. Soc. Am. A* 37 (2020) 284-293. <https://doi.org/10.1364/josaa.37.000284>.

- [58] Q. Sun, E. Klaseboer, A Non-Singular, Field-Only Surface Integral Method for Interactions between Electric and Magnetic Dipoles and Nano-Structures, *Ann. Phys.* (2022) 2100397. <https://doi.org/10.1002/andp.202100397>.
- [59] Q. Sun, K. Dholakia, A.D. Greentree, Optical Forces and Torques on Eccentric Nanoscale Core–Shell Particles, *ACS Photonics* 8 (2021) 1103-1111. <https://doi.org/10.1021/acsp Photonics.0c01825>.
- [60] B. Mortazavi, M. Shahrokhi, M. Makaremi, T. Rabczuk, Anisotropic mechanical and optical response and negative Poisson's ratio in Mo_2C nanomembranes revealed by first-principles simulations, *Nanotechnology* 28 (2017) 115705. <https://doi.org/10.1088/1361-6528/aa5c29>.
- [61] M. R. Query, Optical constants, Available online at <http://www.dtic.mil/docs/citations/ADA158623>, last accessed on Jan 10, 2022.